REPORT DOCUMENTATION PAGE

1a. REPORT SECURITY CLASSIFICATION	1b. RESTRICTIVE MARKINGS

2a. SECURITY CLASSIFICATION AUTHORITY	3. DISTRIBUTION/AVAILABILITY OF REPORT
2b. DECLASSIFICATION/DOWNGRADING SCHEDULE	

4. PERFORMING ORGANIZATION REPORT NUMBER(S)	5. MONITORING ORGANIZATION REPORT NUMBER(S)
219	

6a. NAME OF PERFORMING ORGANIZATION	6b. OFFICE SYMBOL (If applicable)	7a. NAME OF MONITORING ORGANIZATION
Crystal Growth and Materials Testing Associates		

6c. ADDRESS (City, State and ZIP Code)	7b. ADDRESS (City, State and ZIP Code)
6918 Lamont Drive Lanham, MD 20706	

8a. NAME OF FUNDING/SPONSORING ORGANIZATION	8b. OFFICE SYMBOL (If applicable)	9. PROCUREMENT INSTRUMENT IDENTIFICATION NUMBER
Naval Research Laboratory		N00014-86-C-2180

8c. ADDRESS (City, State and ZIP Code)	10. SOURCE OF FUNDING NOS.			
Disbursing Officer Attn: Code 1332 Naval Research Laboratory, Wash., DC 20375-5000	PROGRAM ELEMENT NO.	PROJECT NO.	TASK NO.	WORK UNIT NO.

11. TITLE (Include Security Classification)
Ceramics

12. PERSONAL AUTHOR(S)
R.J. Arsenault, N. Louat, M. Duesbery, R. Spann, S. Lawrence

13a. TYPE OF REPORT	13b. TIME COVERED	14. DATE OF REPORT (Yr., Mo., Day)	15. PAGE COUNT
Final	FROM 8-29-86 TO 2-29-88	1988 Nov. 3	55

16. SUPPLEMENTARY NOTATION

17. COSATI CODES			18. SUBJECT TERMS (Continue on reverse if necessary and identify by block number)
FIELD	GROUP	SUB. GR.	

19. ABSTRACT (Continue on reverse if necessary and identify by block number)

The intrinsic task of this contract was to perform research to obtain fundamental insights into the mechanical and electrical properties of ceramics.

The specific items in the statement of work are necessary steps that had to be completed inorder to reach the goal of obtaining fundamental insights.

In this final report, five topics will be discussed in detail:

∘ Fracture of ceramics ,

∘ Computer modelling of ceramics containing ordered voids ,

∘ Interaction of dislocations with planar free surfaces ,

∘ Application of superconducting ceramics to microwave substrates ,

∘ High T_c superconducting ceramic oxides . (JES)

20. DISTRIBUTION/AVAILABILITY OF ABSTRACT	21. ABSTRACT SECURITY CLASSIFICATION
UNCLASSIFIED/UNLIMITED ☐ SAME AS RPT. ☐ DTIC USERS ☐	

22a. NAME OF RESPONSIBLE INDIVIDUAL	22b. TELEPHONE NUMBER (Include Area Code)	22c. OFFICE SYMBOL
Richard J. Arsenault	301-454-4075	

DD FORM 1473, 83 APR   EDITION OF 1 JAN 73 IS OBSOLETE.

Report No. 219

CERAMICS

Dr. R.J. Arsenault
Director
Crystal Growth and Materials Testing Associates
6918 Lamont Drive
Lanham, Maryland 20706

Project Scientists

Dr. M. Duesbery
Dr. S. Lawrence
Dr. N. Louat
Mr. J. Spann

3 November 1988

Final Report for Contract No. N00014-86-C-2180

Disbursing Office
ATTN: Code 1332
NAVAL RESEARCH LABORATORY
Washington, DC 20375-5000

TABLE OF CONTENTS

SUMMARY

The intrinsic task of contract N00014-86-C-2180 was to per-
form research to obtain fundamental insights into the mechanical
and electrical properties of ceramics.

The specific items in the statement of work are necessary
steps that had to be completed in order to reach the goal of
obtaining fundamental insights.

In this final report five topics will be discussed in detail

- Fracture of ceramics

- Computer modelling of ceramics containing ordered voids

- Interaction of dislocations with planar free surfaces

- Application of superconducting ceramics to microwave
  substrates

- High T_c superconducting ceramic oxides having potential
  applications in electromagnetic equipment and components

Fracture in Ceramics

N. Louat

Measurements of K_{IC} in ceramics are commonly made using channelled specimens in a double cantilever configuration. One difficulty with this method is that the moment necessary for initial crack motion exceeds that which is necessary when it is fully developed and which can be related to the specific properties of the material.

One method of overcoming this difficulty is to modify the specimen geometry so that within certain bounds crack propagation becomes increasingly difficult with increasing crack length. The modification considered here is to make the specimen wedge-shaped in the sense that the channel increases linearly in thickness t, from an initial value t_o, distance x from the free end in the range $o \leq x \leq L$ and is constant and equal to t_m for $x > L$. In order that this procedure be efficacious it is necessary to ascertain the values of L and of t_m/t_o such that is certain that the value of the moment M necessary for the initiation if fracture is insufficient for propagation in the region $x > L$.

As a point of departure we suppose that the stress necessary for crack initiation at the specimen edge to be that found by experiment in simple bend tests and to have the value, σ_T. We have then to compare this with that developed at the same place when moments $\pm M$ associated with the double cantilever configuration are applied. Having fixed M_T as the moment necessary for initiation we have then to determine the specimen bevelling necessary so that $M_T < M_\rho$, where M_ρ is the moment necessary for crack propagation in the parallel sided double cantilever configuration.

Now, the stresses developed near the top of the specimen are sensitive to the manner of application of the bending moments. We suppose this is achieved by the application of loads distributed as shown schematically below in Fig. 1
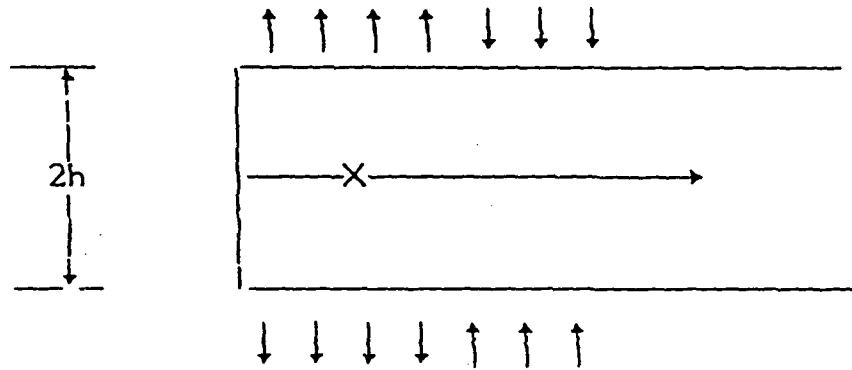

Fig. 1. Schematic load distribution

We suppose that these loads are the same on both faces, to lie in the range $o \leq x \leq a$ and to be distributed according to some function $f(x)$ and that, in order these forces develop only a moment,

$$\int_o^a f(x)\,dx = 0$$

As first approximation we treat the determination of the resultant stresses as a two-dimensional problem in elasticity theory. Here we require that normal and shear stresses vanish over the end surface and take on prescribed values on the top and bottom. Accordingly, we seek a solution of the bi-harmonic equation

$$\frac{\delta^4 \phi}{\delta x^4} + 2\frac{\delta^4 \phi}{\delta x^2 \delta y^2} + \frac{\delta^4 \phi}{\delta y^4} \tag{1}$$

where ϕ represents the Airy stress function. In these terms we may write:

$$\sigma_{xx} = \frac{\delta^2\phi}{\delta x^2}, \quad \sigma_{yy} = \frac{\delta^2\phi}{\delta y^2}, \quad \sigma_{xy} = \frac{\delta^2\phi}{\delta x \delta y}. \tag{2}$$

Now (1) allows for four disposable constants and at least in the case where solutions are available by assuming that the variables are separable we are then able only to specify normal and shear stresses on top and bottom surfaces. Because it is free, normal and shear stresses are to vanish on the edge surface. The solutions envisaged do not in general allow this. However, by adding a dummy section to the specimen so as to have symmetry about the end surface we can eliminate the shear stresses. Proceeding to the solution of this problem we shall see that while the stresses normal to the edge surface do not vanish they are small and that the error in neglecting them is likewise small.

In these terms the general solution of (1) is

$$\phi_m = \cos\frac{m\pi x}{l}\left\{ C_1 \cos h\frac{m\pi y}{l} + C_2 \sin h\frac{m\pi y}{l} \right.$$

$$\left. + C_3 y \cos h\frac{m\pi y}{l} + C_4 y \sin h\frac{m\pi y}{l} \right\} \tag{3}$$

$$\equiv \cos\frac{m\pi x}{l} \cdot f(y)$$

and using the relations (2) we find:

$$C_1 = \frac{2\beta}{\alpha^2} \frac{\sinh\alpha + \alpha h \cosh\alpha h}{\sinh 2\alpha h + 2\alpha h} \tag{4}$$

$$C_2 = C_3 = 0;$$

$$C_4 = -\frac{2\beta}{\alpha^2} \cdot \frac{\alpha \sinh \alpha}{\sinh 2\alpha h + 2\alpha h} \tag{5}$$

$$\alpha = m\pi/l$$

Substituting for C_1 and C_4 from (4) and (5) into (3), we find

$$\sigma_{xx} = 2B \left\{ \frac{(\alpha h \cosh\alpha h - \sinh\alpha h) \cosh\alpha y - \alpha y \sinh\alpha y \sinh\alpha c}{\sin 2\alpha h + 2\alpha h} \right\} \cos\alpha x \tag{6}$$

$$\sigma_{xy} = -2B \left\{ \frac{(\alpha h \cosh\alpha h + \sinh\alpha h) \cosh\alpha y - \sinh\alpha y \sinh\alpha c}{\sinh 2\alpha h + 2\alpha h} \right\} \cos\alpha x \tag{7}$$

$$\sigma_{xy} = -2B \left\{ \frac{\alpha h \cosh\alpha c \sinh\alpha y - \alpha y \cosh\alpha y \sinh \alpha c}{\sinh 2\alpha h + 2\alpha h} \right\} \cos\alpha x \tag{8}$$

Reference to (7) and (8) shows that as required

$$\sigma_{xy} = 0, \sigma_{yy} = -B \cos \frac{m\pi x}{l} ; \quad y = \pm h.$$

This result allows that considerations of a number of solutions such as to match the required value of σ_{yy} on $y = \pm h$. Thus, we consider

$$\bar{\phi} = - \sum_{m=1}^{\infty} B_m \cos \alpha x \cdot f(y)$$

where

$$B_m = \frac{1}{l} \int_{-a}^{a} f(x) \cos \frac{m\pi x}{l} \, dx \tag{9}$$

Then from (7) the required stress $\sigma_M = \sigma_{yy}$ at $x = 0$, $y = 0$ is

$$\sigma_M = - \sum_{m=1}^{\infty} B_m \frac{\alpha h \cosh \alpha h + \sinh \alpha h}{\sinh 2\alpha h + 2\alpha h} \tag{10}$$

This is not the stress which appears at the end of the actual specimen. There, the surface is free. This requires an additional constraint: normal stresses are to vanish (shear stresses vanish already). The vanishing of these stresses involves a displacement of the surface involved. Now displacements which affect σ_{xx} also affect σ_{yy} and in the same way. This is fortunate here because σ_{xx} at $x = 0$, $y = 0$ is from (6)

$$\sum_{1}^{\infty} B_m \frac{\alpha h \cosh \alpha h - \sinh \alpha h}{\sinh 2\alpha h + 2\alpha h} \cdot$$

This is a positive quantity while σ_{yy} is negative. Consequently, surface adjustments which reduce σ_{xx} increase σ_{yy}. Thus, σ_{yy} as given represents an underestimate of the stress actually occurring.

Thus, $M_C > M_I$

where M_C is the moment calculated on this basis as necessary to produce the stress for crack initiation. Thus, in determining a M_p which exceeds M_C we also satisfy

$$M_p > M_I$$

which is what is required.

It then remains to specify $f(x)$. This can be done in a number of ways. Having due regard to the method of attachment between specimen and lever arms, it seems appropriate to take full cognizance of the effect of the specimen bevelling. Thus, the stresses appearing in the loading arms of thickness a when bent under the action of moments M are

$$\frac{M_X}{I} = \frac{M\ (2x-a)}{2I}$$

where X is the distance from the center of inertia of a loading arm and I is the second moment of area about that center. Then taking specimen thickness at a distance x from its end as:

$$t = t_o + (t_m - t_o)\ x/L$$

The stresses in the specimen are

$$\sim \frac{M}{2I}\ (2x - a)\ \frac{aL}{Lt_o + x(t_m - t_o)}$$

Thus (9) becomes

$$B_m = \frac{MaL}{2I} \int_{-a}^{a} \frac{(2x - a)}{Lt_o + x (t_m - t_o)} \cos \frac{m\pi x}{I} dx$$

$$= \frac{MaL}{I} \left\{ \frac{1}{m\pi} \sin \frac{m\pi a}{I} - \frac{aL}{2I} \left[\cos \frac{m\pi B}{I} \left(ci \frac{m\pi}{I} (B+A) - ci \frac{m\pi B}{I} \right) \right. \right.$$

$$\left. \left. + \sin \frac{m\pi B}{I} \left(si \frac{m\pi}{I} (B+A) - si \frac{m\pi B}{I} \right) \right] \right\}$$

with
$$si (x) = \int_{x}^{\infty} \sin t \frac{dt}{t}$$

and
$$ci (x) = \gamma + \ln x + \int_{o}^{x} \frac{\cos t - 1}{t} dt$$

Substitution of this value in (10) gives a final expression for the stresses at the center of the edge of the specimen.

Unfortunately, these series are intractable to analytic summation but they have been readily evaluated numerically by Dr. Duesbery for suitable values of the various parameters. These results show that a particular value of σ_M can be achieved over a range of values of M. This facility allows a check of the authenticity of a measurement of the M necessary for fracture. Thus, the value obtained must lead to the appearance of a stress σ_M which exceeds the fracture stress as measured in a simple bend test on the same material.

COMPUTER MODELLING OF CERAMICS CONTAINING ORDERED VOIDS

M. Duesbery

I. INTRODUCTION

The object of this research was to investigate the fracture properties of lead zirconate titanate (PZT) ceramic.

For many of the mechanical characteristics of ceramic composites, analytic theoretical solutions of the field equations are not obtainable and numerical methods must be used. A reasonable approach to computer simulation can be achieved by adapting standard molecular dynamics techniques[1] using "particles" containing one or more crystal grains in place of molecules and an empirical form fitted to known mechanical and structural properties for the particle-particle interaction[2].

In the linear limit, this particle dynamic (PD) method has been shown[3] to be formally equivalent to the finite element (FE) method used widely for engineering application. However, the PD method has several significant advantages over the FE method for the problem at hand.

(a) Nonlinearities (such as are encountered in the fracture process, for example) are more easily handled using PD methods.

(b) Interactions and constraints additional to the basic cohesive potential are easily incorporated into the PD Hamiltonian formulation. For example, grain boundary energy anistropy can be simulated by superimposing an orientation-dependent modulation on the cohesive term; inhomogeneities and second phases can be incorporated with similar ease.

(c)   The PD method does not require matrix inversion and is consequently more efficient for very large models.

II.   SIMULATIONS OF STRESS DISTRIBUTIONS

Mechanical failure of ceramics usually occurs at fabrication-induced surface flaws which can amplify the applied stress to the failure level.   There are at least two aspects of the stress distribution in ceramics containing void arrays which are relevant to the mechanical performance of PZT transducers, both of which must be evaluated by comparison with void-free material. The first of these is the maximum internal enhancement of an applied stress, which if very large, can lead to intrinsic failure, i.e. failure independent of flaws.   The second factor, which governs the probability of failure at flaws, is the integrated magnitude of the enhancement on exposed stressed surfaces.   For optimum mechanical performance both factors should be minimized.

Internal stress distributions have been calculated for two-dimensional models containing rectangular voids with a variety of sizes and array geometries and deformed within the linear elastic limit to a fixed deflection by three-point bending.   The results suggest that the expected linear superposition of single-void effects is supplemented by cooperative effects due to the regularity of the void lattice.

The modifications induced in the stress field by an isolated void are twofold.   Firstly, the stress distribution is changed to conform to the boundary conditions that there be no normal stresses at the end surfaces of the void.   Secondly, the stresses

in the neighborhood of the void are increased to maintain field equilibrium over the decreased cross-sectional area. There are also stress concentrations at the void corners which are probably due to the sharpness of the corners.

Typical stress distributions when an ordered array of voids is present similarly reflect the void boundary conditions by showing regions of depleted stress in the intervoid regions parallel to the principal tensile stress. Stress concentrations in the uninterrupted tensile fibers are present, due to stress redistribution required for equilibrium. The stress concentrations at the void corners are significantly larger than for isolated voids. It is suspected that this is due to the regular arrangement of voids which causes the model to resemble a two-component system consisting of alternate layers of matrix and matrix-void composite with different effective elastic stiffnesses.

The magnitude of the stress concentrations at the void corners in the 2D models depends strongly on the dimensions of the voids and the array parameters. For example, for voids which are extremely narrow in the principal stress direction, the stress concentrations at the void corners can reach a factor of two larger than the maximum stress encountered in the reference void-free specimen. It has been found empirically that the maximum internal stress shows a strong correlation with the square of the ratio of the intervoid dimensions parallel and normal to the principal stress. Therefore, it is possible to

engineer void arrays which have only minor internal stress enhancements.

A special case occurs when the void array intersects a stressed surface. The stress concentrations at the void corners are similar to those encountered for internal void arrays but the stressed surface, the usual source of ceramic failure, is nearly completely unloaded which means that the surface flaws have been effectively deactivated.

In summary, our two-dimensional modelling has shown that both of the stress distribution factors affecting transducer performance can be influenced significantly by choice of void sizes and array dimensions. The internal stress enhancement cannot be removed, but can be minimized. The integrated surface stresses, on the other hand, can be reduced substantially. Preliminary work on three-dimensional simulations suggests that the effects are less extreme than in two dimensions, i.e. the enhancements and depletions are not as pronounced.

III. SIMULATIONS OF FRACTURE

Another factor which influences the mechanical performance of ceramic transducers is the fracture toughness. In a homogeneous continuum when a crack has been nucleated, propagation can continue unchecked because the crack tip fields, which by definition meet the fracture criteria, are invariant to translation. In a crystalline solid, small modifications are necessary to this general principle because of the discrete structure. However, in a strongly inhomogeneous material, such as a ceramic containing

an array of voids, the process of crack propagation is largely divorced from that of crack nucleation. In practical terms, this means that crack nucleation, although necessary, is not a sufficient condition for fracture failure. It is necessary also that the crack be able to move through the whole sample.

We have modelled failure by fracture for many of the void array configurations considered in Section II, considering both flaw-free models and models containing a controlled flaw. Novel fracture processes have been observed which have improved our understanding of the fracture-mediating properties of void arrays.

For flaw-free models it has been found that fracture always begins at the location of the largest tensile stress. This position in most cases is at a void corner adjacent to the tensile surface or at the tensile surface immediately below a void. In the first case, the crack moves from the void corner to the surface and is effectively blunted; in the second case, motion is from surface to void with the same blunting. In both cases the crack has been arrested and further propagation proceeds from void to void, but only at an increased applied stress. Only when the void separation in the direction parallel to the principal stress is very large does crack propagation proceed through the matrix without arrest at voids.

The preference for crack propagation to proceed by this void "unzipping" mechanism has been demonstrated further by simulations in models with a controlled flaw located at the center of

the tensile surface. The flaw is simulated by breaking a bond between two surface particles, thereby creating an extrinsic stress concentration. The stress at the tip of the flaw is enhanced to a level typically 15-20% greater than the most highly stressed void corners, but crack nucleation still occurs preferentially at the void corners and proceeds by the same unzipping mechanism.

In summary, fracture in two-dimensional models containing void arrays is observed to proceed preferentially by a void unzipping mechanism with crack arrest and renucleation at higher applied stress at each stage. Crack propagation between voids is strongly inhibited by the low level of stored elastic energy in the inter-void regions. These phenomena combine for suitable void array geometries to provide an intrinsic means for increasing fracture toughness of ceramics.

References

1.   M.S. Duesbery and M. Kahn, submitted to J. Amer. Ceram. Soc.

2.   W.G. Hoover, "Molecular Dynamics," Lecture Notes in Physics, Springer-Verlag, NY, 1986.

3.   W.T. Ashurst and W.G. Hoover, "Microscopic Fracture Studies in the Two-Dimensional Triangular Lattice," Phys. Rev. B14 (1976) 1465.

ON THE INTERACTIONS OF DISLOCATIONS WITH
PLANAR FREE SURFACES

N.P. Louat and K. Sadananda*

Abstract

Fourier synthesis is employed to obtain solutions to the coupled singular integrations which according to the method of dislocation continua represent equilibrium.

The cases of screw and edge dislocations totally contained within parallel planar surfaces are considered first. An initial extension of the method to problems in three dimensions is then made and exemplified by the treatment of an edge dislocation which lies normal to a free surface.

Introduction

The stress fields of dislocations which lie parallel to infinite free surfaces have been evaluated in a number of ways [1,2,3,4]. Among these is the representation of the conditions for equilibrium of a single surface in terms of singular integral equations. This method is here further developed so as to deal with cases where more than one face surface can be involved and where the dislocation is not parallel to a single surface. To illustrate the method and recover known results we begin with the simple case of a screw dislocation in a thin plate.

1. Screw Dislocation Totally Within a Thin Plate

We consider a elastically isotropic plate of thickness h, with a screw dislocation located at a distance y from the lower surface. The stresses

---

* Employee, Material Science and Technology Div., NRL

at a point of coordinates η, ζ referred to this dislocation are:

$$\sigma_{z\zeta} = \frac{\mu b}{2\pi} \frac{\eta}{y^2 + \zeta^2} \tag{1}$$

$$\sigma_{zy} = \frac{\mu b}{2\pi} \frac{\zeta}{y^2 + \zeta^2}$$

where μ is the shear modulas and b the Burgers vector.

We now suppose that the stress-engendered surface displacements can be represented by the distribution of a dislocation continuum in each surface. We designate the distributions of lower and upper surfaces as $\alpha(x)$ and $\beta(x)$, respectively.

For this situation, the stresses σ_{yz} must vanish at the free surfaces. We represent these conditions in terms of the dislocation continua through the singular integral equations:

$$\frac{x}{x^2 + y^2} = \int_{-\infty}^{\infty} \alpha(t) \frac{dt}{t-x} + \int_{-\infty}^{\infty} \beta(t) \frac{t-x}{(t-x)^2 + h^2} dt; \tag{2}$$

$$\frac{x}{x^2 + (h-y)^2} = \int_{-\infty}^{\infty} \beta(+) \frac{dt}{t-x} + \int_{-\infty}^{\infty} \alpha(+) \frac{t-\eta}{(t-x)^2 + h^2} dt. \tag{3}$$

Towards the solution of these simultaneous equations we suppose:

$$\alpha(x) = \int_{0}^{\infty} A(k) \cos kx \, dk; \tag{4}$$

$$\beta(x) = \int_0^\infty \beta(k) \cos kx \, dk. \tag{5}$$

and note that

$$\frac{x}{x^2+y^2} = \int_0^\infty e^{-ky} \sin kx \, dk.$$

Then substituting in (2) and (3) we have

$$\int_0^\infty e^{-ky} \sin kx \, dk = \int_0^\infty A(k) \, dk \int_{-\infty}^\infty \cos kt \, \frac{dt}{t-x}$$

$$+ \int_0^\infty B(k) \, dk \int_{-\infty}^\infty \cos kt \, \frac{t-x}{(t-x)^2+h^2} \, dt$$

$$= -\pi \int_0^\infty A(k) \sin kx \, dk - \pi \int_0^\infty B(k) e^{-kh} \sin kx \, dk$$

and similarly

$$\int_0^\infty e^{-k(h-y)} \sin kx \, dk = -\pi \int_0^\infty B(k) \sin kx \, dk - \pi \int_0^\infty A(k) e^{-kh} \sin kx \, dk$$

Whence,

$$e^{-ky} = -\pi A - \pi B e^{-kh};$$

$$e^{-k(h-y)} = -\pi B - \pi A e^{-kh}.$$

Solving these simultaneous linear equations we have:

$$A = -\frac{1}{\pi}\frac{\sinh k(h-y)}{\sinh kh}; \qquad B = \frac{1}{\pi}\frac{\sinh ky}{\sinh kh}.$$

Then using (4) and (5),

$$\beta(x) = -\frac{1}{2h}\frac{\sin \pi y/h}{\cos \pi x/h + \cos \pi y/h};$$

$$\alpha(x) = -\frac{1}{2h}\frac{\sin \pi y/h}{\cos \pi x/h - \cos \pi y/h}.$$

The stresses τ_{zy} developed by these arrays are at the point $\bar{\eta}$, ζ (reference lower surface):

$$\int_{-\infty}^{\infty} \alpha(x)\frac{x-\bar{y}}{(x-\bar{y})^2+\zeta^2} + \beta(x)\frac{x-\bar{y}}{(x-\bar{y})^2+(h-\bar{\zeta})^2}\, dx$$

$$= -\frac{1}{2\pi}\sin\frac{\pi y}{h}\int_{-\infty}^{\infty}\left\{\frac{1}{\cosh\frac{\pi x}{h}-\cos\frac{\pi y}{h}}\cdot\frac{x-\bar{y}}{x-\bar{y}+\zeta^2} + \frac{1}{\cosh\frac{\pi x}{h}+\cos\frac{\pi y}{h}}\cdot\right.$$

$$\left.\frac{x-\bar{y}}{(x-y)^2+(h-\zeta)^2}\right\}\, dx \qquad (6)$$

This is readily evaluated by considering the contour integral

$$\oint \frac{1}{\cos z\pi/h-\cos\pi y/h}\,\frac{dz}{z-\bar{\eta}-i\bar{\zeta}}; \qquad z = u+iv$$

with the contour consisting of the planes $v = o$ and $v = h$, joined at infinity by vertical lines. This contour is to be transversed in the positive (anti-clockwise) direction so that the two infinite integrals are transversed in opposite directions and so have opposite signs. This is compensated for by the fact that $\cosh \pi \ (u+i\ h)/h = \cosh \pi u/h$. In turn, the real parts of $1/(z-\eta-i\zeta)$ are the required algebraic functions of (6). Using Cauchy's residue theorem the required integral is thus the real part of

$$\frac{\mu b}{2\pi} \cdot 2\pi i \left\{ \frac{1}{\cosh \pi \ \bar{\eta}+i\zeta/h \ -\cos \pi y/h} \right\}$$

$$= -\frac{\mu b}{2h} \left\{ \frac{\sinh \frac{\pi \bar{\zeta}}{h} \cdot \sin \frac{\pi \bar{\eta}}{h} \cdot \sin \frac{\pi y}{h}}{\left(\cosh \frac{\pi \bar{\eta}}{h} \cos \frac{\pi \zeta}{h} - \cos \frac{\pi y}{h} \right)^2 + \sinh^2 \frac{\pi \bar{\zeta}}{h} \sin^2 \frac{\pi \bar{\eta}}{h}} \right\}$$

This agrees with the result from a single plane when $h \rightarrow \infty$.

2. Edge Dislocation Totally Within a Thin Plate

Proceeding as for the case of the screw dislocation we consider a plate of thickness h, with an edge dislocation with its Burgers vector, b, parallel to the surfaces located at a distance y from the lower surface. The stresses at a point of coordinates x, η referred to this dislocation are:

$$\sigma_{xy} = \psi \times \frac{(x^2-y^2)}{(x^2+y^2)^2} ; \tag{7}$$

$$\sigma_{yy} = \psi \, y \, \frac{(x^2-y^2)}{(x^2+y^2)^2} \tag{8}$$

$$\sigma_{xx} = -\psi \, y \, \frac{(3x^2+y^2)}{(x^2+y^2)^2} \tag{9}$$

where $\psi = \mu b / 2\pi (1-\nu)$.

Proceeding as before we now suppose that the surface displacements engendered by these stresses can be represented by two distributions of dislocation continua in each surface. The displacement vectors of each pair are mutually orthogonal, being either parallel or perpendicular to the surfaces. We designate the distributions of the lower surface as $f(t)$ and $g(t)$ and those of the upper surface by $h(t)$ and $k(t)$. The displacement vectors of $f(t)$ and $h(t)$ are chosen to be parallel to the surfaces.

With these definitions and using (7), (8) and (9) we formulate the equations of equilibrium: lower surface (shear stresses vanish);

$$\psi \, x \, \frac{(x^2-y^2)}{(x^2+y^2)^2} \;=\; A \int_{-\infty}^{\infty} f(t) \, \frac{dt}{t-x} + A \int_{-\infty}^{\infty} h(t)\,(t-x) \, \frac{(t-x)^2 - h^2}{[(t-x)^2 + h^2]^2} \, dt$$

$$+ \, A \int_{-\infty}^{\infty} k(t) \, h \, \frac{h^2 - (t-x)^2}{[(h^2 + (t-x)^2)^2]^2} \, dt$$

where $A = \mu\lambda / 2\pi(1-\nu)$ and λ represents the magnitude of a unit dislocation; upper surface (shear stresses vanish);

$$\psi y \frac{(x^2-y^2)}{(x^2+y^2)^2} = -A \int_{-\infty}^{\infty} f(t) \frac{dt}{t-x} + Ah \int_{-\infty}^{\infty} h(t) \frac{(t-x)^2-h^2}{[(t-x)^2+h^2]^2} dt$$

$$+ A \int_{-\infty}^{\infty} k(t)(t-x) \frac{3h^2+(t-x)^2}{[h^2+(t-x)^2]^2} dt$$

Lower surface (normal stresses vanish);

$$\psi y \frac{(x^2-y^2)}{(x^2+y^2)^2} = -A \int_{-\infty}^{\infty} g(t) \frac{dt}{t-x} + Ah \int_{-\infty}^{\infty} h(t) \frac{(t-x)^2-h^2}{[(t-x)^2+h^2]^2} dt$$

$$+ A \int_{-\infty}^{\infty} k(t)(t-x) \frac{3h^2+(t-x)^2}{[h^2+(t-x)^2]^2} dt. \qquad (12)$$

Upper surface (normal stresses vanish);

$$\psi(h-y) \frac{x^2-(h-y)^2}{[x^2+(h-y)^2]^2} = -A \int_{-\infty}^{\infty} k(t) \frac{dt}{t-y} - Ah \int_{-\infty}^{\infty} f(t) \frac{(t-x)^2-h^2}{[(t-x)^2+h^2]^2} dt$$

$$+ A \int_{-\infty}^{\infty} g(t)(t-x) \frac{3h^2+(t-x)^2}{[(t-x)^2+h^2)]^2} dt \qquad (13)$$

Having regard to the known parity of the functions involved, we now suppose that:

$$f(t) = \int_0^\infty F(k) \cos kt \, dk;$$

$$h(t) = \int_{-o}^\infty H(k) \cos kt \, dk;$$

$$g(t) = \int_0^\infty G(k) \sin kt \, dk;$$

$$k(t) = \int_0^\infty K(k) \sin kt \, dk.$$

Then taking (as appropriate) the sine and cosine transforms of the left-hand-side of equations (4-7), these become

$$\int_{-\infty}^\infty (1-ky) e^{-ky} \sin kx \, dx = \int_{-\infty}^\infty \frac{dt}{t-x} \int_0^\infty F(k) \cos kt \, dk$$

$$+ \int_{-\infty}^\infty (t-x) \frac{(t-x)-h^2}{[(t-x)^2+h^2]^2} dt \int_0^\infty H(k) \cos kt \, dk$$

$$+ h \int_{-\infty}^\infty \frac{h-(t-x)^2}{[h^2+(t-x)^2]^2} dt \int_0^\infty K(k) \sin kt \, dk$$

$$= \pi \int_0^\infty F(k) \sin kx \, dk + \pi \int_0^\infty (1-kh) e^{-kh} H(k) \sin kx \, dk$$

$$+ \pi h \int_0^\infty k e^{-kh} K(k) \sin kx \, dk$$

and so

$$\frac{1}{\pi}(1-ky)e^{-ky} = F(k) + \pi(1-kh)e^{-kh}H(k) + \pi hk\,e^{-kh}K(k)$$

In like manner (5), (6) and (7) become

$$\frac{1}{\pi}[1-k(h-y)]e^{-k(h-y)} = H(k) + (1-kh)e^{-kh}F(k) - khe^{-kh}G(k)$$

$$-\frac{1}{\pi}ky\,e^{-ky} \qquad = -G(k) + (1+kh)e^{-kh}K(k) - kbe^{-kh}H(k)$$

$$\frac{1}{\pi}k(h-y)e^{-k(h-y)} \qquad = -K(k) + (1+kh)e^{-kh}G(k) + kh\,e^{-kh}F(k)$$

Thus, the system of simultaneous integral is reduced to four linear algebraic equation in the Fourier transforms. The solution of these equations is straightforward, but tedious and easily subject to error. In practice, the use of algebraic computer programs is recommended. The solutions found by hand are:

$$\pi(c^2-1)^2 F(k) = -E(c^2-1-a+J-Jc^2-ac^2) - DC(1+2a-c^2-d+c^2d);$$

$$\pi(c^2-1)^2 G(k) = E(J-c^2J-c^2a-a) + DC(dc^2-d+2a);$$

$$\pi(c^2-1)^2 H(k) = -Ec(Jc^2-c^2-J+1+2a) - D(-de^2+c^2-1-a+d-ac^2)$$

$$\pi(c^2-1)K(k) = -Ec(Jc^2-J+2a) - D(d-c^2d-ac^2-a).$$

where: $E = e^{ky}$; $J = k(h-y)$; $D = e^{k(h-y)}$; $c = e^{kh}$; $a = kh$ and $d = ky$.

Thus, for example:

$$F = 2\frac{(e^{kh}-1)e^{kh}(\sinh k(y-h) + ky \cosh k(y-h) - 4khe^{2kh}\sinh ky}{\pi(e^{2kh}-1)^2} \quad \ldots$$

Similar expressions are obtained for G, H and K.

The stresses at a point x_0, y_0 are then given by integration. For example, the contribution to the shear stresses σ_{xy} from the distribution G are seen to be:

$$\sigma_{xy}(G) = y_0 \int_{-\infty}^{\infty} \frac{y_0^2 - (x-x_0)^2}{\{y^2 + (x-x_0)^2\}^2} \, dx \int_0^{\infty} G(k) \sin kx \, dk \tag{15}$$

where

$$g(x) = \int_0^{\infty} G(k) \sin kx \, dk$$

Changing the order of integration we have

$$\sigma_{xy}(G) = y_0 \int_0^{\infty} G(k) \, dk \int_{-\infty}^{\infty} \frac{(y_0^2 - u^2)}{(y_0^2 + u^2)^2} \sin k(u+x) \, du$$

$$= y_0 \int_0^{\infty} G(k) \, dk \int_0^{\infty} \frac{(y_0^2 - u^2)}{(y_0^2 + u^2)^2} \cos ku \sin kx \, du$$

$$= -\frac{\pi}{2} y_0 \int_0^{\infty} G(k) \sin kx \, k \, e^{-ky} \, dk \tag{16}$$

The integrals resulting from substitutions such as that necessary for G(k) in (16) do not appear to be effectable in terms of known functions. However, numerical integration can be expected to be a simple matter.

3. Edge Dislocation Normal to a Free Surface

Here we are concerned with a surface which must for our purposes be represented as two-dimensional rather than one. Accordingly, we represent the displacements necessary to achieve a stress free surface as an assembly of elementary dislocation loops having Burgers vectors which are normal to the surface and lie in the z-direction.

Following Kroupa[5] the relevant stress due a small loop of area Δ and displacement vector $\bar{\lambda}$ is at a radius R from the center of the loop is:

$$\sigma_{zz} = \frac{\Delta\bar{\lambda}\mu}{4\pi(1-v)R^3} \equiv \frac{K\Delta\bar{\lambda}}{R^3}$$

Then taking the stress σ_{zz} at a point x,y in the surface (z-o) due an edge dislocation with Burgers vector b lying in the y-direction as:

$$\sigma_{zz} = \frac{\mu b(1+\nu)}{\pi(1-\nu)} \cdot \frac{x}{x^2+y^2}$$

we have for equilibrium:

$$K \int_0^\infty dt \int_0^\infty \frac{f(t,v)\,dv}{[(x-t)^2+(y-v)^2]^{3/2}} + \frac{\mu b(1+\nu)}{\pi(1-\nu)} \frac{x}{x^2+y^2} = 0. \qquad (18)$$

Here, μ is the shear modulus and ν the Poisson's ratio and we have adopted the convention that the stresses from loops with a layer of inserted material are positive. $f(t,v)$ represents the displacement vector of the loop at the point distant t,v from the dislocation and consequently the surface displacement there. Eliminating constants, (18) becomes

$$\int_0^\infty dt \int_0^\infty \frac{f(t,v)\, dv}{[(x-t)^2+(y-v)^2]^{3/2}} + \frac{\mu b(1+\nu)}{\pi(1-\nu)} \frac{x}{x^2+y^2} = 0$$

We now proceed somewhat as before but using double Fourier transforms so that we can write

$$4b(1+\nu) \frac{x}{x^2+y^2} = \frac{8b(1+\nu)}{\pi} \int_0^\infty \int_0^\infty \frac{k}{k^2+s^2} \sin ks \cos sy \, dk \, ds.$$

and on introducing the Fourier transform $F(k,s)$ and changing the order of integrations

$$\int_0^\infty \int_0^\infty F(k,s)\, dk \, ds \int_0^\infty \int_0^\infty \frac{\sin kt \cos sv}{[(x-t)^2+(y-v)^2]^{3/2}} \, dt \, dv$$

$$= 4b(1+\nu) \int_0^\infty \int_0^\infty \frac{k}{k^2+s^2} \sin kx \cos sy \, dk \, ds$$

Substituting: $x-t = u$; $y-v = w$, the first expression reduces to

$$\int_0^\infty \int_0^\infty F(k,s) \sin kx \cos sy \, dk \, ds \int_0^\infty \int_0^\infty \frac{\cos sw \cos ku}{(u^2+w^2)^{3/2}} \, du \, dw \qquad (19)$$

Now, it may be observed that the second set of integrals are not well behaved. This difficulty may be handled following Hadamard[6] and taking the finite part. Thus, we write

$$\int_0^\infty \frac{\cos sw}{(u^2+w^2)^{3/2}}\, dw = \frac{1}{u}\frac{d}{du}\int_0^\infty \frac{\cos sw}{(u^2+w^2)^{\frac{1}{2}}}\, dw$$

$$= \frac{2}{u}\frac{d}{du} K_0 (s_1 u)$$

where K_0 is a complete elliptic function of the first kind. Thus,

$$\int_0^\infty \cos ku\, du \int_0^\infty \frac{\cos sw\, dw}{(u^2+w^2)^{3/2}} = -2s \int_0^\infty \frac{K_1(su) \cos ku}{u}\, du$$

$$= 2 \int_0^\infty dk \int_0^\infty s\, K_1(su)\, \sin ku\, du$$

$$= \pi \int_0^\infty \frac{k\, dk}{(s^2+k^2)^{\frac{1}{2}}} = \pi\,(s^2+k^2)^{\frac{1}{2}}$$

Substituting in Eq. 19, we have ..

$$\pi \int_0^\infty \int_0^\infty F(k,s)\,(s^2+k^2)^{\frac{1}{2}} \sin kx \cos sy\, dk\, ds$$

$$= 4b(1+\nu) \int_0^\infty \int_0^\infty \frac{k}{k^2+s^2} \sin kx \cos sy\, dk\, ds$$

so that $F(k,s) = \dfrac{4b}{\pi}(1+\nu)\dfrac{k}{(k^2+s)^{3/2}}$

and

$$f(t,v) = \int_0^\infty \int_0^\infty F(k,s) \sin kt \cos sv \, dk \, ds$$

$$= \frac{4b(1+\nu)}{\pi} \int_0^\infty \int_0^\infty \frac{k}{(k^2+s)^{3/2}} \sin kt \cos sv \, dk \, ds$$

$$= \frac{4b(1+\nu)}{\pi} \int_0^\infty t \, K_0(t\lambda) \cos sv \, ds$$

so that

$$f(t,v) = b(1+\nu) \frac{t}{(t^2+v^2)^{\frac{1}{2}}} \; .$$

Thus, the displacement at a distance r from the dislocation is sinusoidal with rotation about the dislocation. It is a maximum at the position of the inserted or (missing) plane of atoms.

Now, Kroupa has given all the stresses σ_{xx}, σ_{xy}, σ_{yy} due to an infinitisimal loop as a function G of the coordinates x, y and z so that the stresses arising from the free surface are immediately expressible in terms of integrals of the form

$$\int_0^\infty \int_0^\infty f(t,v) \, G \, (x-t, y-v, z) \, dt \, dv$$

Development of this approach to deal with straight dislocations skew to the surface appears realizable but Kroupa's expressions appear so

complicated that the task of dealing with two parallel surfaces is, to say the least, daunting.

SUMMARY

It has been shown that certain problems involving the displacements of free surfaces in the presence of dislocations can be expressed in terms of coupled integral equations and that they can be reduced to ordinary simultaneous algebraic equations in the Fourier transforms of the unknown functions. Three problems are detailed: (1) a screw and (2) an edge dislocation totally within a thin plate and (3) an edge dislocation normal to a free surface.

REFERENCES

1.   A.K. Head, Froc Phys. Soc., **66B**, (1953) 801.

2.   N.P. Louat, Nature **196** (1962) 1081.

3.   F.R.N. Nabarro and C.J. Kostlan, J. Appl. Phys. **49** (1978) 5445.

4.   W. Moss and J. Hoover, J. Appl. Phys. **49** (1978) 5449.

5.   F. Kroupa, Phil. Mag. **7** (1962) 783.

6.   J. Hadamard, Lectures on Cauchy's Problem, Dover Publ., 139.

APPLICATION OF SUPERCONDUCTING CERAMICS TO MICROWAVE SUBSTRATES

R. Spann and M. Kahn*

ABSTRACT

The following is a status report on work directed towards the attainment of superconducting, high performance microstrip transmission lines, using $YBa_2Cu_3O_{7-x}$ (YBC) material.

Section I describes efforts at qualifying the composition and preparation process of superconducting powder. This was characterized in superconductive discs by X-ray analysis, resistance-temperature behavior and microstructure. In Section II, preparation parameters of adherent, graded layers of superconducting YBC material on alumina are discussed.

I. INTRODUCTION

It has been shown that localized voids can significantly enhance the signal propagation rates in microstrip transmission lines[1], without affecting the desired thermal properties of the substrates. This also opens avenues to reducing problems such as crosstalk between closely spaced conductor paths, as well as making possible tailored delay lines where paths of physically different lengths can have the same propagation delay.

Superconductors repulse external magnetic fields. The electromagnetic coupling between two adjacent microstrip transmission lines is therefore eliminated and crosstalk is further reduced. The absence of series resistance in the strip line can also be expected to further minimize the

---

* Employee of the Material Science and Technology Division, NRL

pulse dispersion. Preparation parameters of superconductive film strip lines·on ceramics containing voids as well as the modelling of their behavior are to be addressed.

II. BACKGROUND AND OBJECTIVES

The demonstrated increases in pulse propagation rates of microstrip transmission lines on ceramics with patterned voids were attained by a topical reduction of the dielectric constant of the substrate, implemented through the application of fugitive ink and tape technology. Hybrid technology was then applied to print the conductors.

It is the primary aim of the present work to investigate the materials, processes and technology needed to make these conductors superconductive, so as to further enhance the high speed pulse performance of these micro-circuits.

III. FILM DEPOSITION APPROACHES

The application of superconductive films to ceramic substrates containing void patterns was evaluated by using two approaches:

1. Submicron thick films result from the pyrolytic decomposition of organometallic solutions. Three to five such layers can result in films 2 μm thick. Conductors, 0.5 mm wide, made from such films could carry only about 1 mA before superconductivity is lost. The preparation of much thicker films from organometallic material does not appear practical at this time.

2. Films, 20 to 80 μm thick, can easily be made by using conventional "thick film" technology. "Conventionally" prepared ceramic powders were

used for this and deposition via the thick film process was investigated in depth.

SECTION 1 SELECTION AND CHARACTERIZATION OF MATERIALS SYSTEM

As a first step, it is necessary to qualify the chemical composition and determine the proper physical parameters of a ceramic powder that will give a patternable and adherent film. It has to be superconducting at the temperature of liquid nitrogen and must be able to be handled without damage or loss of properties.

Preliminary studies have therefore concentrated on materials preparation, and on microstructural and physical characterization of the resulting *superconducting powders.* These were initially evaluated by pressing them into discs and testing their properties after suitable heat treatment.

A. POWDER PREPARATION

High temperature superconducting $YBa_2Cu_3O_{7-x}$ (YBC) ceramic powders were prepared from barium carbonate[a], yittria[b] and copper[c] oxides. In a related experiment, barium fluoride or copper fluoride were used as a source of fluorine to flux the formulation and/or to substitute for some of the oxygen in the lattice (References 2,3,4).

To prepare the powders, stoichiometric quantities of predried $BaCO_3$, Y_2O_3 and CuO were mixed and ground with a mortar and pestle. In order

---

(a) Baker CP, Lot H168 or 10146, or Johnson Mathey 14341B, 99.9%, Lot 15506.
(b). Cerac Y-1037, or Johnson Mathey 11181c, Batch R3529.
(c) Baker CP, Lot 52647, or Johnson Mathey 10700, Batch S96022.

to achieve uniform mixing, the large grain copper oxide had to be pre-ground in a spex mixer for approximately 20 min. The mixture was then calcined in air at 900-950°C for a total of 6-12 hours, with intermediate grindings with a mortar and-pestle every 1-2 hours. Following the calcination, the powders were either quenched to room temperature or cooled in air at a rate of 0.5-1.0°C per min. and ground for use. They were then evaluated by X-ray diffraction.

B. DISC PREPARATION

Two approaches were used for the preparation of ceramic discs for the evaluation of the powders. In one approach, discs ~ 2.5 cm in dia. by 3-6 mm thick were vacuum hot pressed at 25-30 MPa and 950°C. For this, either dry mixed precursors or the calcined powder was used. These discs were then heat treated in oxygen at 950-975°C for 36-64 hours and cooled slowly at a rate of 0.5-1.0°C per min. to below 400°C. In some experiments, a 1-3 hour hold at 500-700°C was used to more fully oxygenate the product.

Alternatively, discs 1.2-1.7 cm in dia. by 3-6 mm thick were prepared by cold pressing the powder at 80-100 MPa. The compacts were then heat treated at ~ 950°C for 12-64 hours, followed by the above cooling rate in flowing oxygen.

C. RESULTS

The oxidation state of the YBC compound controls the degree of super-conductivity. Thermogravimetric analysis (Jay Wallace[5]) has shown that at around 400°C this material begins to lose oxygen and that the rate of this loss increases as the temperature is raised. The phase diagram[6]

furthermore indicates that at about 1020°C, any localized excess of barium that may be present contributes to the formation of a melt. Upon resolidification of the melt, other phases will be formed rather than the tetragonal or the orthorhombic YBC compound and as a result the loss of oxygen appears then to be irreversible.

After the processing parameters were determined, two 50g lots of powder were prepared. The powder in sample 8-27-1 (see Table I) was cooled slowly in air following the calcining treatment while that in the sample 10-08-2 was quenched to room temperature. The slow cooling resulted in a mixture of tetragonal and orthorhombic phases. A typical X-ray diffraction trace for such mixed material is shown in Fig. 1. Rapidly cooled powder had a tetragonal structure with an X-ray pattern as shown in Fig. 2. However, after cold pressing, sintering and annealing, both powders gave ceramic bodies that were primarily orthorhombic (See Fig. 3). These results agree closely with those shown in Ref. 7. These observations suggest that it is not necessary to start with an orthorhombic powder in order to produce a ceramic superconductor. After annealing, the majority of these cold pressed samples exhibited a sharp drop to almost zero resistance between 90 and 95 K as well as a strong Meissner effect when coooled in liquid nitrogen. The latter indicates that at least 50% of the material had a superconducting phase.

Hot pressing was performed in a graphite die under a mechanically pumped vacuum. The hot pressed material exhibited none of the X-ray peaks normally found in either tetragonal or orthorhombic YBC. However, after extended annealing, an orthorhombic structure and a Meissner effect

were observed. Densities were below 73%. The substitution of 2 wt.% barium fluoride in the matrix depressed the compaction, i.e. densification, temperature in the hot press from 950°C to below 900°C, but a significant amount of residual $BaCuO_2$ in the annealed samples was detected using X-ray diffraction. Nevertheless, the structure was orthorhombic and there was some Meissner effect. Additions of CuF_2 gave similar results, except that in this case BaF_2 peaks were found to emanate both from the calcine as well as from the sintered material. Hot pressing of uncalcined precursors that contained BaF_2 showed residues of $BaCO_3$, $BaCuO_2$ and Y_2O_3, attributable to an incomplete reaction in the non-superconductive fraction of the material.

Some typical resistance temperature curves are shown in Fig. 4. Higher fluorine concentrations appear to depress the slope of the resistance vs. temperature curve in the normal state. They also seem to lower the transition temperature and introduce a phase having a finite resistivity below the transition temperature.

Additional characterization of the superconducting material pertained to its microstructural as well as to the appearance of individual crystallites in the matrix. The polished surface of a disc which was examined under visible light is shown in Fig. 5. Note the irregularly shaped pores in the micrograph. The shapes of these pores is significantly different than those of pores resulting from "normal", i.e. solid state diffusion controlled, pore growth. The sharp corners observed imply that final formation takes place late in the sintering process, under lower temperature annealing conditions. Vapor transport processes which may take place during the lower

temperature oxygen exchange reaction may enhance this.

The grains vary in size from 5 to 25 μm and have a significant range of contrasts. Crystal twins appear on many of the polished surfaces. Such twinning has been seen before (Ref. 8, 9, 10) and details can be observed in the dark field TEM micrograph in Fig. 6. An amorphous grain boundary layer, about 30 μm thick, can be seen in the bright field TEM micrograph in Fig. 7. The effect of these grain boundaries on the maximum current density of the superconductor will be investigated.

SECTION 2   METHODOLOGY FOR THE PREPARATION OF SUPER-CONDUCTIVE LAYERS ON ALUMINA SUBSTRATES

A. EXPERIMENTAL

The powders used for this work were from the two 50g batches of $YBa_2Cu_3O_{7-x}$ powder, samples 8-27-1 and 10-08-2 as discussed in Section I. These were made from a precalcined, undoped stoichiometric YBC composition. For the layer deposition, they were mixed into a paste that contained either 50% of A10 PMMA or a mix of .15% elvacite, .15% acetone and 70% mineral spirits. After thorough mixing, these pastes were printed onto the as-fired surface of an alumina substrate. The samples were then brought to temperature in a tube furnace with oxygen flow at ambient pressure, held at that temperature and then cooled as detailed.

B. Results

The results from these experiments are discussed in Table II. the specific heat treatments and some of the observations made on the YBC

layers are shown there. The degree of interaction of the film with the substrate is of initial concern. Too much interaction could result in excess alumina diffusion and contamination of the superconductive layer, but as sample A in Table II shows, the reaction of the relatively coarse powder with the substrate was low. Acceptable adhesion of the powder to the substrate was attained only when a peak temperature of 975°C was held for 30 minutes (See sample E). Even then, the film was very porous and had limited interparticle cohesion. When finer powder was used for this interfacial layer, the expected stronger adhesion and smoother surface were obtained but only with the higher peak temperature heat treatment. On the other hand, the layer from the finer powder showed considerable aggregation and was more reduced even after only 5 minutes at 975°C. This was attested by its more tetragonal X-ray diffraction pattern (See sample J in Table II.).

To improve the continuity of the YBC layers and their surface smoothness, a second layer of powder was deposited and fired over these layers. This also served to eliminate the effects of any substrate material that may have diffused into the base layer from the top of the substrate.

The last item in Table II represents an initial experiment with two separately fired YBC layers. It showed some improvement in cohesion and a somewhat less rough external surface. To obtain a suitable finer powder for the deposition of a smooth second layer, the YBC powder was screened, mixed with an equal weight of toluene and milled for 24 hours in a plastic container. The ZrO_2 milling media used showed some weight loss (0.6% of that of the powder) but the resulting fine YBC powder was

well dispersed and seems to give a smooth texture second layer. The as-milled powder exhibited numerous extraneous diffraction peaks, but after one hour at temperatures as low as 100°C, the original typical YBC diffraction pattern was reestablished.

IV. SUMMARY

The conditions required to produce a powder for superconducting coatings have been identified. The best precursors were $BaCO_3$, Y_2O_3 and premilled CuO calcined at 950°C. The best method of heat treatment was found to involve firing to 950°C and cooling slowly in oxygen.

It is indicated that layers of superconductive material can be fired onto sintered alumina without getting detrimental substrate interaction and diffusion. An adequate amount of adhesion to the substrate can nevertheless be maintained at the same time.

It also appears that two layers, using different particle size YBC powder will provide an expeditious approach toward attaining the desired properties.

REFERENCES

1. M. Kahn, C. Scott, "Patterned Voids in Microstrip Transmission Lines," Proc. 1987 Fall Meeting, Amer. Ceram. Soc.

2. B.E. Walker, Jr., R.W. Rice, R.C. Pohanka and J.R. Spann, "Densification and Strength of $BaTiO_3$ with LiF and MgO Additives," Bull. Am. Ceram. Soc., $\underline{E55}$ (3) 274-278 (1976).

3. B.E. Walker, R.W. Rice and J.R. Spann, "High Strength Barium Titanite Ceramic Bodies," U.S. Pat. 3,753,911 (1973).

4. B.E. Walker, R.W. Rice and J.R. Spann, "Strengthened and High Density $BaTiO_3$," U.S. Pat. 3,862,046 (1975).

5. J. Wallace, private communication (1987).

6. Phase diagram, NBS.

7. W. Wong, -Ng and L.P. Cook, "X-ray Studies of Helium-Quenched $Ba_2Cu_3O_{7-x}$," Adv. Ceram. $\underline{2}$ (3B) 624-631 (1987).

8. B. Bender, L. Toth, J.R. Spann, S. Lawrence, J. Wallace, D. Lewis, M. Osofsky, W. Fuller, E. Skelton, S. Wolf, S. Quadri and D. Gubser. "Processing and Properties of the High Tc Superconducting Oxide Ceramic," Ad. Cera. Mat. $\underline{2}$ (3B) 506-511 (1987).

9. L.E. Toth, M. Osofsky, S.A. Wolf, S.B. Quadri, W.W. Fuller, D.U. Gubser, J. Wallace, C.S. Pande, A.K. Singh, S. Lawrence, W.T. Elam, B.Bender and J.R. Spann, "Processing of High Temperature Ceramic conductors: Structure and Properties," Chemistry of a High Temperature Superconductor, Ed. D.L. Nelson, W.S. Whittingham and T.F. George, ACS Symp. Series 351 (Chap 221) 228-239, Amer. Chem. Soc., Wash., DC (1987).

10. R. Beyers, G. Lim, E.M. Engler, R.J. Savoy, T.M. Shaw, T.R. Dinger, W.J. Gallagher and R.L. Sandstrom, "Crystallography and Microstructure of $YBa_2Cu_3 O_{9-x}$, A Perovskite-Based Superconducting Oxide," Appl. Phys. Ltrs., submitted for publication, 1987.

FIGURES

1. X-ray diffraction tract typical of that from a rapidly cooled calcine, diffraction tract typical of that from a rapidly cooled calcine, suggesting the presence of both tetragonal and orthorhombic crystals.

2. X-ray pattern typical of tetragonal $YBa_2Cu_3O_{6.5}$ crystals. Note the reversal of peaks at $\sim 47^0$ and $\sim 58^0$ from those shown in Fig. 3.

3. Typical X-ray diffraction pattern of calcine or a disk after annealing. The double peaks at $\sim 32.5^0$, $\sim 47^0$, $\sim 58^0$ are typical of orthorhombic $YBa_2Cu_3O_7$.

4. Resistance vs. temperature curves of YBC composition with a range of fluorine concentrations.

5. Optical (cross polarized light) micrograph of polished surface of $YBa_2Cu_3O_{7-x}$ showing porosity, grain size and twinning.

6. Dark field TEM micrograph of $YBa_2Cu_3O_{7-x}$ showing twinning.

7. Bright field (A) TEM micrograph showing a thin amorphous grain boundary phase between two grains of $YBa_2Cu_3O_{7-x}$.

TABLE I

Results of Powder Evaluation

Sample	Additive	Pressing Temp.	Calcine Cooling Rate	Calcine X-ray Results	Annealed Disc X-ray results	Meissner Effect
8-27-1	None	250C	Slow	Orthorhombic + Tetragonal	Orthorhombic, $BaCuO_2$	Good
10-08-2	None	250C	Fast	Tetragonal	Orthorhombic	Good
4-27-1	None	950C	Fast	Orthorhombic	Orthorhombic	Good
9-29-1	24% BaF_2	250C	Slow	Orthorhombic + Tetragonal	Orthorhombic, $BaCuO_2$	Good
5-06-1a	2% BaF_2	950C		Uncalcined precursors	Orthorhombic, $BaCO_3, Y_2O_2$	Good

Table II

Sample	Particle (Screen) Size	Tmax (°C)	Tmax (min)	Time at Cooling (hrs.)	Adhesion[2]	Cohesion	Surface Appearance	Equiv. Quench. Temp.[1]	Residual Phases	Comments
8-27-1	<75μm	960	30	>16 hrs	Slight	Slight	Rough	600°C	$BaCuO_2$	
8-27-1	<75μm	975	30	3 hrs.	Good	Slight	Rough	700°C	$BaCuO_2$	
10-8-2	>75μm	975	30	3 hrs.	Good	Slight	Rough			
M-19	Submicron	975	5	3 hrs.	Strong	Slight	Smooth + aggregates	750°C	$BaCuO_2$	64 hrs. 411°C anneal
8-27-1	<75μm	975	5	3 hrs.	Strong	Some	Coarse	650	$BaCuO_2$	Two separate fired layers

[1] Quenching temperature of YBC compound that has been shown elsewhere (7) to generated x-ray diffraction patterns most similar to that of sample. 400°C gives the most orthorhombic x-ray patterns.

[2] Slightly: Powder comes off with scotch tape.
Some: Some powder comes off with knife.
Good: Powder comes off with knife with difficulty.
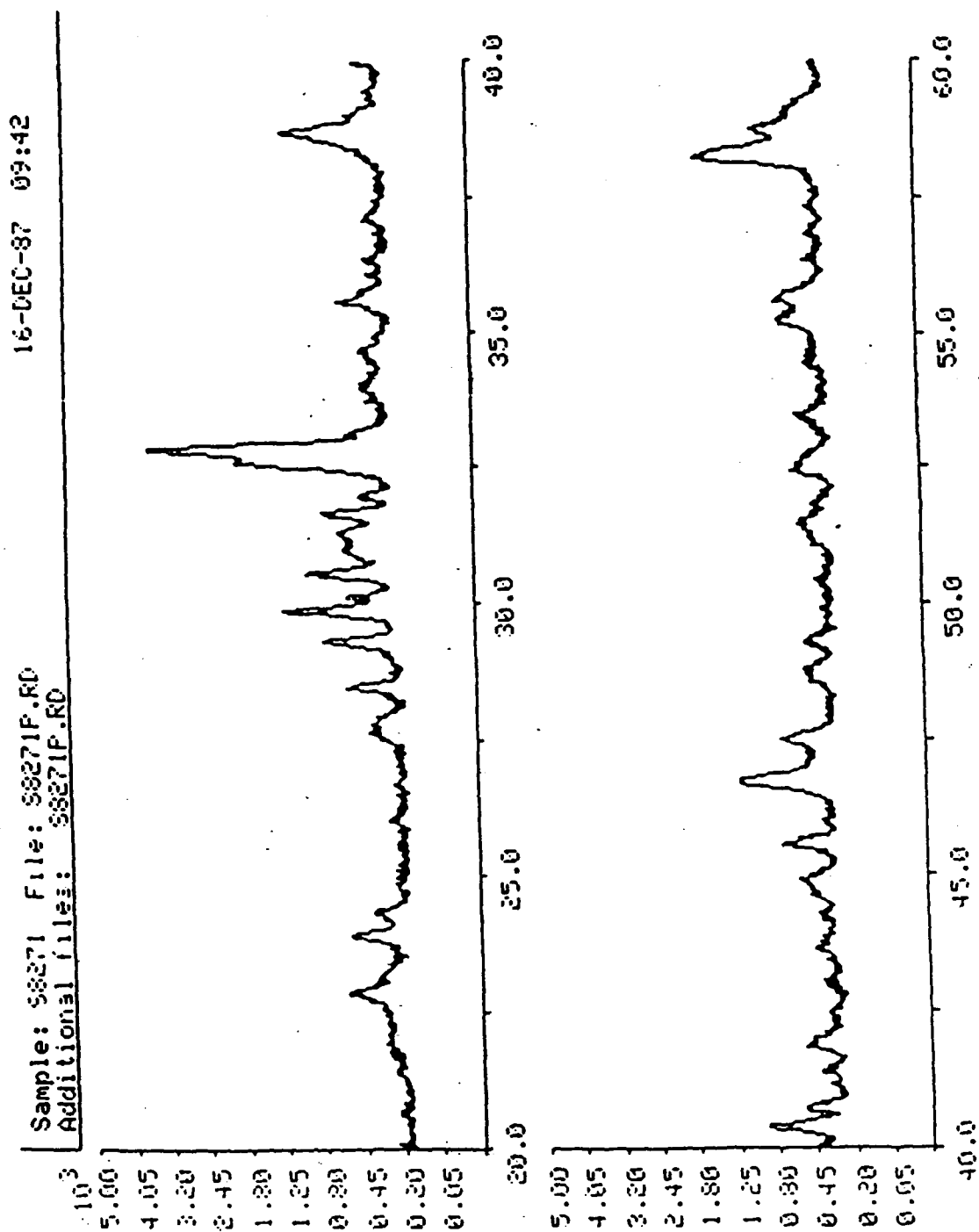Strong: Powder almost impossible to remove.

43

Fig. 1. X-ray diffraction trace typical of that from a rapidly cooled calcine, suggesting the presence of both tetragonal and orthorhombic crystals.
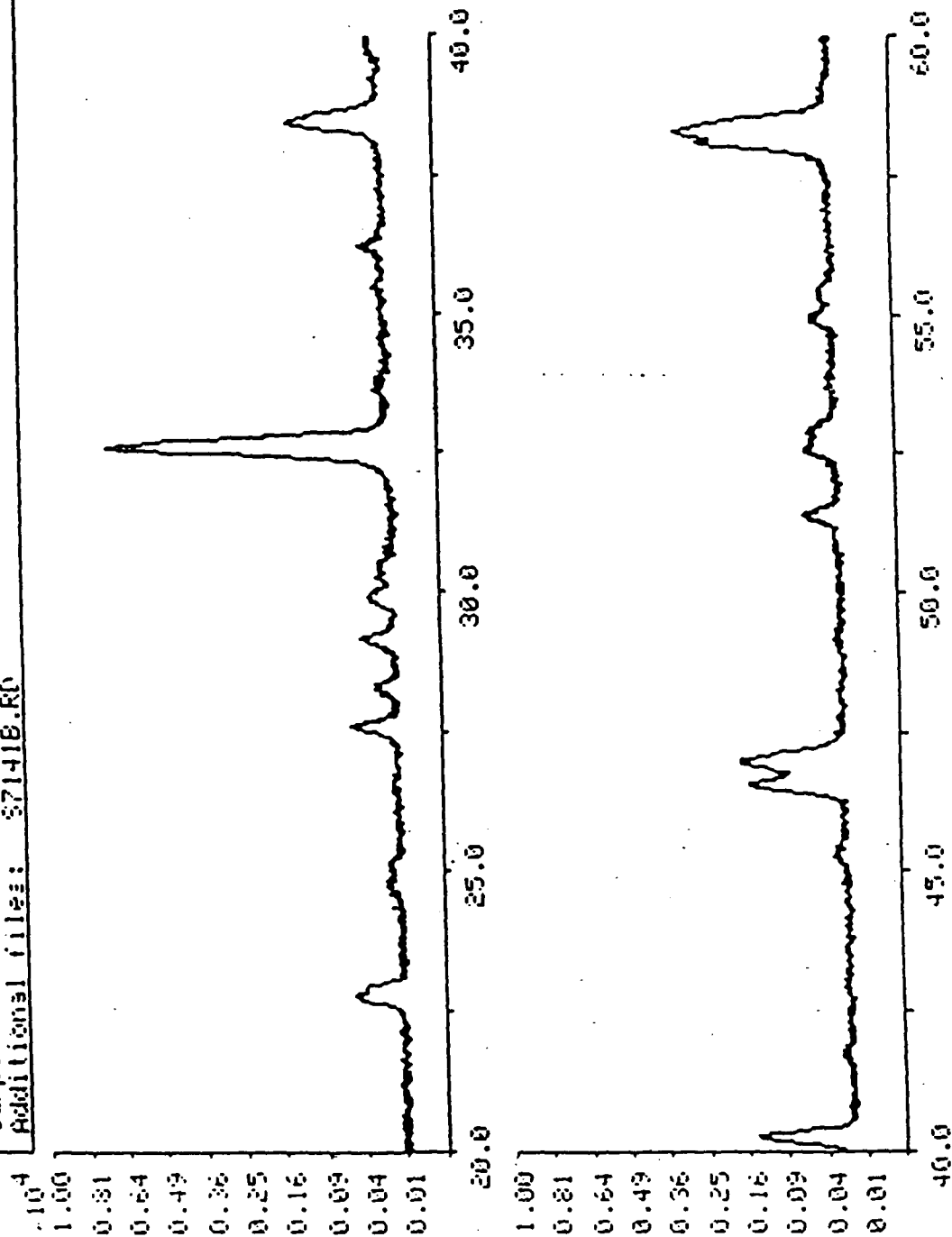
Sample: S7141 File: S7141B.RO
Additional files: S7141B.RO

16-DEC-87 09:33

Fig. 2. X-ray pattern typical of tetragonal YBa$_2$Cu$_3$O$_{6.5}$ crystals. Note the reversal of peaks at ~47° and ~58° from those show in Figure 3.
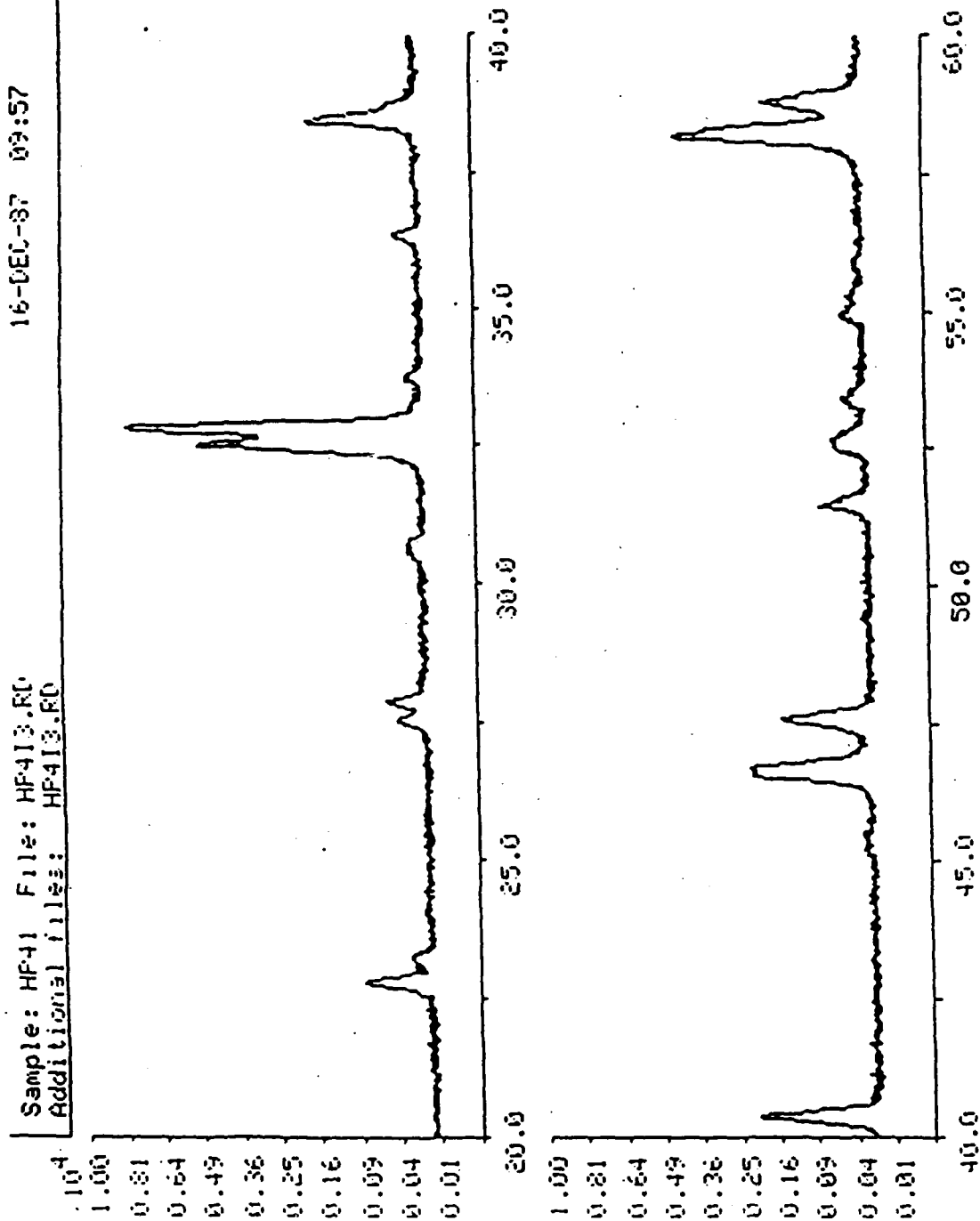
Fig. 3. Typical x-ray diffraction pattern of calcine or a disk after annealing. The double peaks at ~ 32.5°, ~ 47° ~ 58° are typical of orthorhombic $YBa_2Cu_3O_7$.
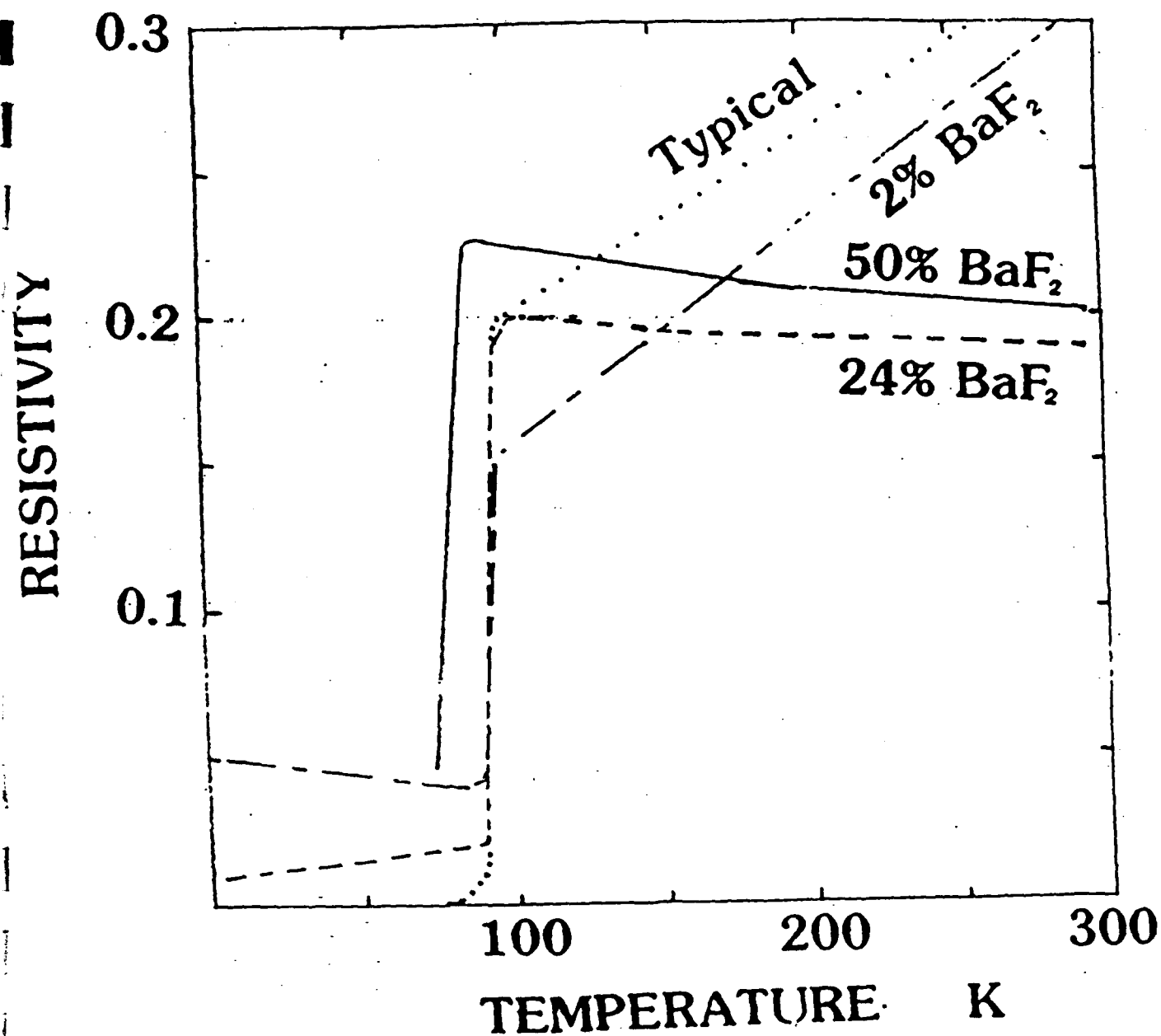
Fig. 4. Resistance versus temperature curves of YBC composition with a range of fluorine concentrations.
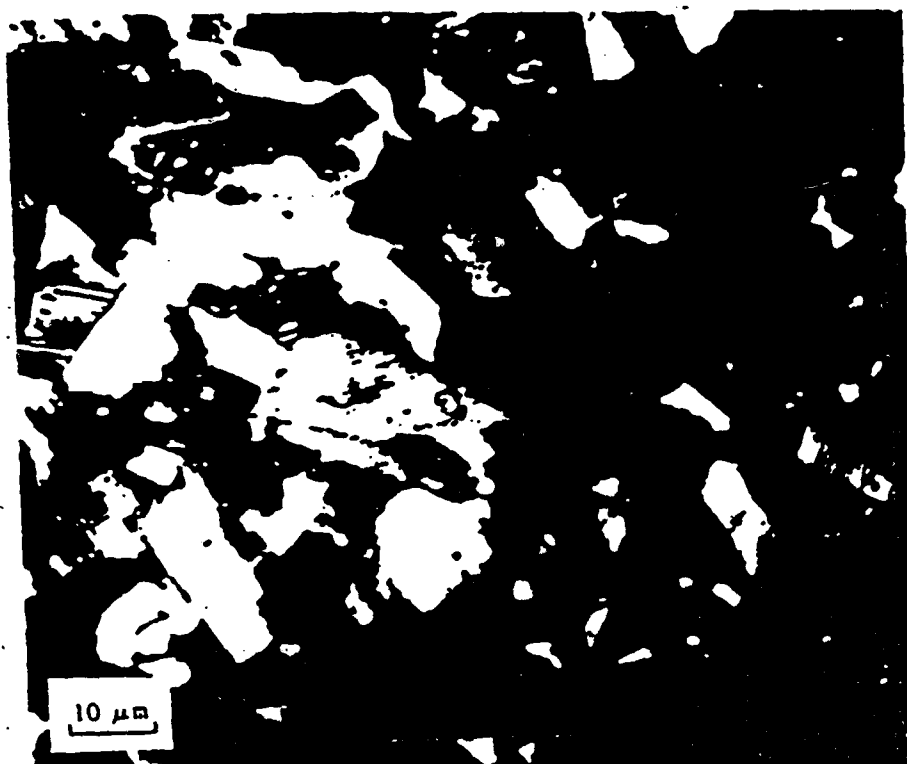
Fig. 5. Optical (cross polarized light) micrograph of polished surface of $YBa_2Cu_3O_{7-x}$ showing porosity, grain size and twinning.
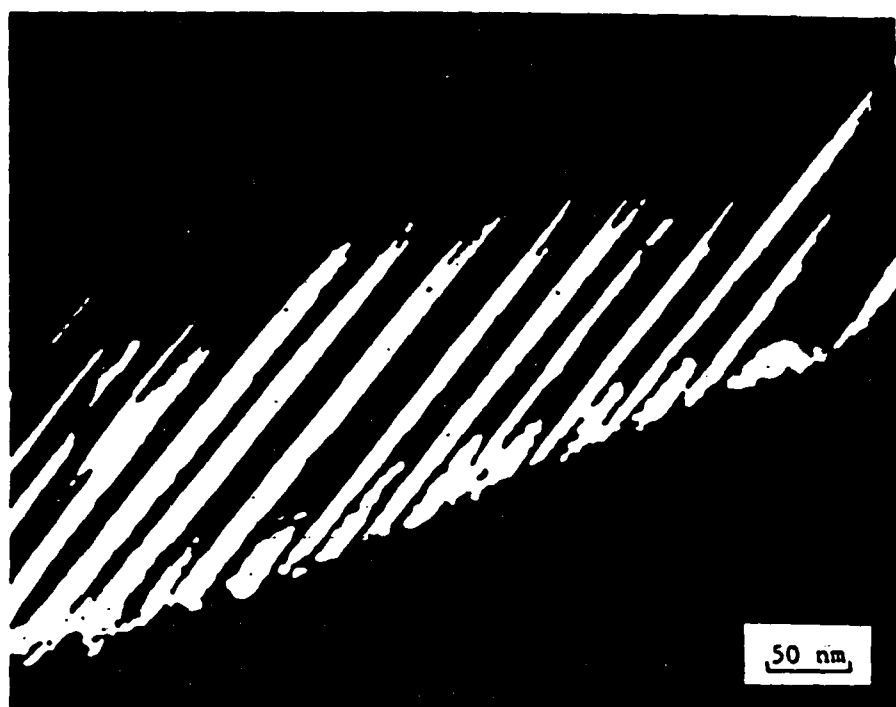
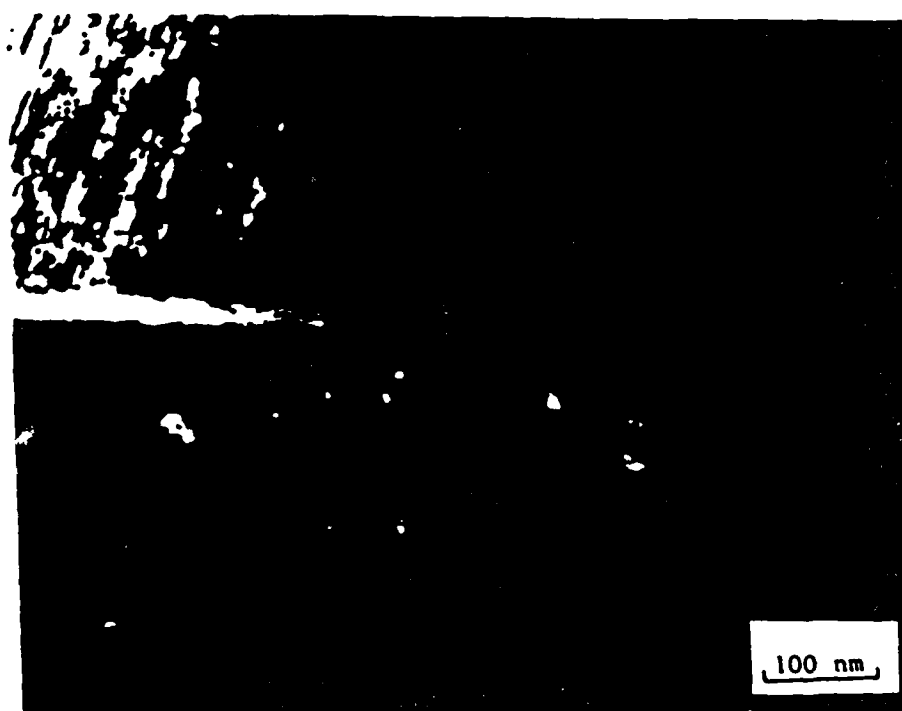Fig. 6. Dark field TEM micrograph of $YBa_2Cu_3O_{7-x}$ showing twinning.

Fig. 7. Bright field (A) TEM micrograph showing a thin amorphous grain boundary phase between two grains of $YBa_2Cu_3O_{7-x}$.

RESEARCH AND DEVELOPMENT OF HIGH T_C SUPERCONDUCTING CERAMIC OXIDES HAVING POTENTIAL APPLICATIONS IN ELECTROMAGNETIC EQUIPMENT AND COMPONENTS

S.H. Lawrence

INTRODUCTION

With the report (1) in late 1986 of superconducting ceramic oxides having record high critical temperature (T_c) values, renewed interest was opened in both the fields of superconductor research and research on ceramic materials for electronic applications. One line of studies concerned itself with the synthesis and properties of the newly discovered class of oxide ceramic superconductors, including their electrical and magnetic properties, as well as their environmental stability. However, because these materials, with T_c values ranging from 35K to 50K, still required the use of liquid helium as the cryogenic refrigerant in order to attain these very low temperatures, most of the continued research was devoted toward discovering new materials which would have even higher T_c values, thereby allowing greater flexibility and simplified engineering considerations to be employed in their practical applications. Such a class of materials was subsequently reported in 1987 (2). While these materials ($Ba_2RCu_3O_7$, R=most rare earth elements; R=Y was used in the work summarized in this report), like the earlier superconductors, require cryogenic conditions to achieve superconductivity (vide infra), they achieve this state at 90K to 95K, thereby permitting the replacement of liquid helium by liquid nitrogen, a much cheaper and more readily obtainable refrigerant. It is anticipated that the successful application of this material, and others which may be subsequently discovered, will revolutionize electronics in general, and with respect to the work reported here, will greatly facilitate the disign of a "low temperature test facility for magneti-resistive materials requiring cryogenic conditions" (see Summary of Work).

SYNTHESIS AND PROPERTIES OF $La_{2-x}M_xCuO_{4-(x/2)+z}$

$[M = Ba, Sr, Ca; 0.1 < x < 0.3; 2 < x < 3; z = (n/2)-1]$

Work on this class of compounds primarily involved varying the alkaline ion (M^{2+}) and the value of x, as well as the processing temperature and time at temperature. The samples were synthesized from La_2O_3, MCO_3 and CuO, which were mixed and ground together, calcined at 1000°C with several intermediate grindings of the calcine, uniaxially cold-pressed to approximately 20,000 psi, and sintered in air or oxygen-overnight at 950-1050°C. The samples with the highest transition temperatures (T_c = 35-40K) were obtained for M = Ba or Sr, and x = 0.10-0.15. In general, it was noted that T_c increases as a function of the value of c/a, where a and c are the unit cell parameters. It was also noted that the intermediate grindings were very necessary in order to maximize exposure of the reactant powder to oxygen and to allow facile escape of carbon dioxide from the decomposition of $BaCO_3$ or $SrCO_3$.

The potential use of this class of oxide ceramics in any low temperature test facility is limited by at least three factors. Firstly, like most ceramics, these materials are brittle and therefore not readily amenable to use in environments requiring mechanical shock resistance. Also, while the T_c values for these materials are higher than anything previously discovered, they would still require liquid helium as a refrigerant, since other readily available refrigerants boil at considerably higher temperatures. Finally, these materials are highly moisture sensitive, apparently due to the high content of La_2O_3; sample pellets left in air were found to crumble after 2 days, with the concomitant formation of $La(OH)_3$. This makes water vapor condensation on these materials, which occurs when they are cooled to superconducting temperatures in air, a serious problem to consider.

SYNTHESIS AND PROPERTIES OF $Ba_2YCu_3O_7$

With the 1987 report of the title compound having $T_c>90K$, work was devoted to this material, since it has a T_c greater than the normal boiling point of liquid nitrogen (77K). It is normally made by calcining Y_2O_3, $BaCO_3$ and CuO at 940°C for at least 4 hours, with intermediate grindings if necessary, followed by pressing and sintering the resulting calcine at 940°C in oxygen for at least 2 hours, followed by slowly cooling or annealing (400-700°C) in oxygen for at least 8 hours. While this procedure usually gives a product having good phase purity, it poses several problems. In the first place, the barium carbonate decomposes at very high temperatures (T>875°C); since YBC ($Ba_2YCu_3O_7$) decomposes at temperatures just above 940°C, there is not much room left for error, and the product powder is large-grained and not readily comminuted. In addition, barium compounds react with nearly all commonly available crucible materials at the requisite processing temperatures. Finally, YBC does not undergo densification readily, even if it is isostatically pressed as a fine powder.

An apparent partial solution to these problems seemed to require the use of a barium oxide precursor which would decompose to the oxide at a temperature lower than $BaCO_3$, in conjunction with identifying conditions of temperature, time at temperature and atmosphere which would permit reaction sintering from the chosen starting materials. What was discovered, in collaboration with Dr. Jay Wallace and Mr. Barry Bender of NRL, was that $Ba(OH)_2 \cdot H_2O$ was a practical and acceptable substitute for $BaCO_3$. It decomposes at 100-150°C less than $BaCO_3$ under comparable conditions, and while it reacts with atmospheric CO_2, the reaction occurs slowly enough to permit its use in air, as long as minimal precautions are taken for its storage. In addition, it was discovered that CuO produced by heating basic copper carbonate, $Cu_2(OH)_2CO_3$ (malachite), produces a powder finer than commercially available CuO.

The use of $Ba(OH)_2 \cdot H_2O$, malachite-derived CuO and Y_2O_3, with reaction conditions using low total pressure of pure oxygen (approximately 50 torr O_2) was found to yield a high density, fine-grained material after the starting materials were reaction sintered. Work is continuing to optimize the superconducting properties of this material.

REFERENCES

1. J.G. Bednorz and K.A. Mueller, "Possible High T_c Superconductivity in the Ba-La-Cu-O System," Zeitschrift fur Physik B 64, 189-193 (1986).

2. M.K. Wu, J.R. Ashburn, C.J. Torng, P.H. Hor, R.L. Meng, L. Gao, Z.J. Huang, Q. Wang, and C.W. Chu, "Superconductivity at 93K in a New Mixed Phase Y-Ba-Cu-O Compound System at Ambient Pressure," Physical Review Letters 58, 908 (1987).

54

PUBLICATIONS AND PRESENTATIONS[*]

1. "High T_c Oxide Ceramic Superconductors: The Research Effort at NRL," S.H. Lawrence, L.E. Toth, B.A. Bender, M. Osofsky, S. Wolf, E. Skelton, D. Gubser, Special Session on High Tc Superconductor Oxides, 1987 National Meeting of the American Ceramic Society, Pittsburgh, PA, April 29, 1987.

2. "Superconducting Phase Transitions in the La-M-Cu-O Layered Perovskite System, M = La, Ba, Sr, and Pb," D.U. Gubser, R.A. Hein, S.H. Lawrence, M.S. Osofsky, D.J. Schrodt, L.E. Toth, and S.A. Wolf, Phys. Rev B 35, 5350 (1987).

3. "Temperature Dependent X-Ray Studies of the High T_c Superconductor $La_{1.9}Ba_{0.1}CuO_4$," E.F. Skelton, W.T. Elam, D.U. Gubser, S.H. Lawrence, M.S. Osofsky, L.E. Toth, and S.A. Wolf, Phys. Rev. B 35, 7140 (1987).

4. "X-Ray Identification of the Superconducting High T_c Phase in the Y-Ba-Cu-O System," S.B. Qadri, L.E. Toth, M. Osofsky, S. Lawrence, D.U. Gubser, and S.A. Wolf, Phys. Rev. B 35, 7235 (1987).

5. "Processing and Properties of the High T_c Superconducting Oxide Ceramic $YBa_2Cu_3O_7$," B. Bender, L. Toth, J.R. Spann, S. Lawrence, J. Wallace, D. Lewis, M. Osofsky, W. Fuller, E. Skelton, S. Wolf, S. Qadri and D. Gubser, Advanced Ceramic Materials 2(3B), 506 (1987).

6. "Structural Considerations of Cu-Oxide Based High-T_c Superconductors," E.F. Skelton, S.B. Qadri, B.A. Bender, A.S. Edelstein, W.T. Elam, T.L. Francavilla, D.U. Gubser, R.L. Holtz, S.H. Lawrence, M.S. Osofsky, L.E. Toth, and S.A. Wolf, High Temperature Superconductors, D.U. Gubser and M. Schluter, editors (Materials Research Society Extended Abstract EA-11, Materials Research Society, Pittsburgh, PA), 161 (1987).

7. "Processing of High-Temperature Ceramic Superconductors: Structure and Properties," L.E. Toth, M. Osofsky, S.A. Wolf, E.F. Skelton, S.B. Qadri, H.W. Fuller, D.U. Gubser, J. Wallace, C.S. Pande, A.K. Singh, S. Lawrence, W.T. Elam, B. Bender, and J.R. Spann, Chemistry of High-Temperature Superconductors (ACS Symposium Series 351), American Chemical Society, Washington, DC, 1987, pp. 228-239.

8. "Phonon Density of States of Superconducting $YBa_2Cu_3O_7$ and the Nonsuperconducting Analog $YBa_2Cu_3O_6$," J.J. Rhyne, D.A. Neumann, J.A. Gotaas, F. Beech, L. Toth, S. Lawrence, S. Wolf, M. Osofsky, and D.U. Gubser, Phys. Rev. B 36, 2294 (1987).

9. "Experimental Program on High T_c Oxide Superconductors at the Naval Research Laboratory," M. Osofsky, L.E. Toth, S. Lawrence, S.B. Qadri, A. Shih, D. Mueller, R.A. Hein, W.W. Fuller, F.J. Rachford, E.F. Skelton, T. Elam, D.U. Gubser, S.A. Wolf, J.A. Gotaas, J.J. Rhyne, R. Kurtz, and R. Stockbauer, High Temperature Superconductors, D.U. Gubser and M. Schluter, editors (Materials Research Society Extended Abstract EA-11, Materials Research Society, Pittsburgh, PA), 173 (1987).

10. "Magnetic Field Studies of the $La_{2-x}M_xCuO_4$ and $Ba_2Y_1Cu_3O_7$ High Tc Superconductors," W.W. Fuller, M.S. Osofsky, L.E. Toth, S.B. Qadri, S.H. Lawrence, R.A. Hein, D.U. Gubser, T.L. Francavilla, and S.A. Wolf, Proc. XVIII Internat. Conf. Low Temp. Phys. (LT18), Kyoto, Japan, 1987.

11. "Preparation, Structure, and Magnetic Field Studies of High T_c Superconductors," M.S. Osofsky, W.W. Fuller, L.E. Toth, S.B. Qadri, S.H. Lawrence, R.A. Hein, D.U. Gubser, S.A. Wolf, C.S. Pande, A.K. Singh, E.F. Skelton and B.A. Bender, Novel Superconductivity, S. Wolf and V. Kresin, editors (Proceedings of the International Workshop on Novel Mechanisms of Superconductivity, June 22-26, 1987, Berkeley, California), 807-815 (1987).

* From work done during the period covered by this report.